Key Points:
- Mean kappa values measured in outflows exceed those predicted by an altitude-dependent entrainment model
- Refractive index is lower aloft (> 8 km versus < 4 km) in nonstorm conditions with high statistical significance, unlike on storm days with inflow and outflow data
- Enhanced hygroscopicity coincides with lower organic mass fraction, higher sulfate mass fraction, and higher O:C ratios of organic aerosol

Correspondence to:
A. Sorooshian,
armin@email.arizona.edu

Contrasting aerosol refractive index and hygroscopicity in the inflow and outflow of deep convective storms: Analysis of airborne data from DC3

Armin Sorooshian[1,2] (iD), T. Shingler[3,4], E. Crosbie[3,4] (iD), M. C. Barth[5] (iD), C. R. Homeyer[6] (iD), P. Campuzano-Jost[7] (iD), D. A. Day[7] (iD), J. L. Jimenez[7] (iD), K. L. Thornhill[3,8] (iD), L. D. Ziemba[3] (iD), D. R. Blake[9], and A. Fried[10] (iD)

[1]Department of Chemical and Environmental Engineering, University of Arizona, Tucson, Arizona, USA, [2]Department of Hydrology and Atmospheric Sciences, University of Arizona, Tucson, Arizona, USA, [3]Chemistry and Dynamics Branch, National Aeronautics and Space Administration Langley Research Center, Hampton, Virginia, USA, [4]Universities Space Research Association, Columbia, Maryland, USA, [5]National Center for Atmospheric Research, Boulder, Colorado, USA, [6]School of Meteorology, University of Oklahoma, Norman, Oklahoma, USA, [7]Cooperative Institute for Research in Environmental Sciences and Department of Chemistry and Biochemistry, University of Colorado Boulder, Boulder, Colorado, USA, [8]Science Systems and Applications, Inc., Hampton, Virginia, USA, [9]Department of Chemistry, University of California, Irvine, California, USA, [10]Institute of Arctic and Alpine Research, University of Colorado Boulder, Boulder, Colorado, USA

Abstract We examine three case studies during the Deep Convective Clouds and Chemistry (DC3) field experiment when storm inflow and outflow air were sampled for aerosol subsaturated hygroscopicity and the real part of refractive index (n) with a Differential Aerosol Sizing and Hygroscopicity Probe (DASH-SP) on the NASA DC-8. Relative to inflow aerosol particles, outflow particles were more hygroscopic (by 0.03 based on the estimated κ parameter) in one of the three storms examined. Two of three "control" flights with no storm convection reveal higher κ values, albeit by only 0.02, at high altitude (> 8 km) versus < 4 km. Entrainment modeling shows that measured κ values in the outflow of the three storm flights are higher than predicted values (by 0.03–0.11) based on knowledge of κ values from the inflow and clear air adjacent to the storms. This suggests that other process(es) contributed to hygroscopicity enhancements such as secondary aerosol formation via aqueous-phase chemistry. Values of n were higher in the outflow of two of the three storm flights, reaching as high as 1.54. More statistically significant differences were observed in control flights (no storms) where n decreased from 1.50–1.52 (< 4 km) to 1.49–1.50 (> 8 km). Chemical data show that enhanced hygroscopicity was coincident with lower organic mass fractions, higher sulfate mass fractions, and higher O:C ratios of organic aerosol. Refractive index did not correlate as well with available chemical data. Deep convection is shown to alter aerosol radiative properties, which has implications for aerosol effects on climate.

1. Introduction

Atmospheric aerosol particles and their interactions with radiation, water vapor, and clouds represent the largest source of uncertainty in current estimates of the total anthropogenic radiative forcing budget [*Intergovernmental Panel on Climate Change*, 2013]. This is partly owing to the short residence time and spatial heterogeneity of particles in the atmosphere, in addition to uncertainty in their properties as a function of age in the atmosphere. Knowledge of vertically resolved aerosol properties in the atmosphere is particularly important for calculations of radiative transfer and cloud processes, in addition to interpretation and use of remote sensing data. One such process that can alter the abundance and properties of aerosol as a function of altitude is convective transport of aerosol particles and gases from the planetary boundary layer (PBL) to the upper troposphere (UT) [e.g., *Pickering et al.*, 1990; *Jaeglé et al.*, 1997; *Huntrieser et al.*, 2002, 2011; *Ridley et al.*, 2004; *Singh et al.*, 2007; *Ancellet et al.*, 2009; *Avery et al.*, 2010; *Barret et al.*, 2010]. Deep convective storms can redistribute aerosols (and gases), process them via aqueous-phase chemistry, and remove them by wet scavenging processes [e.g., *Barth et al.*, 2007, 2016; *Chakraborty et al.*, 2015; *Yang et al.*, 2015; *Bela et al.*, 2016; *Corr et al.*, 2016; *Fried et al.*, 2016].

Measurements of aerosol particles around deep convective storms are challenging, and consequently, uncertainties exist as to how aerosol properties vary between inflow and outflow areas. A complication

in understanding these changes is that entrainment of cloud-free air into the storm influences the convected particles [e.g., *Pickering et al.*, 1992]. One study has shown that the passage of a mesoscale convective system (MCS) resulted in reduced aerosol concentration, enhanced contributions from inorganic constituents (i.e., sulfate, nitrate, and chloride) to total aerosol mass concentrations, and enhanced cloud condensation nuclei (CCN) activity, as quantified by the ratio of CCN to total condensation nuclei (CN) number concentration [*Crumeyrolle et al.*, 2008]. They concluded with support from model simulations that the storm potentially helped add a soluble coating around dust particles that increased their hygroscopicity. Other works have also shown that dust can become coated with more hygroscopic constituents such as sulfate as a result of cloud processing [*Levin et al.*, 1996; *Wurzler et al.*, 2000; *Desboeufs et al.*, 2001; *Yin et al.*, 2002; *Sullivan et al.*, 2007; *Sorooshian et al.*, 2013]. The results of *Crumeyrolle et al.* [2008] were based on airborne measurements before and after the passage of a single MCS, and their measurement of hygroscopicity (CCN:CN) was sensitive to the aerosol size distribution [e.g., *Wonaschütz et al.*, 2013; *Crosbie et al.*, 2015]. Therefore, additional measurements of aerosol properties before and after convective processing are needed, including measurements that are insensitive to the shape of the size distribution.

The Deep Convective Cloud and Chemistry (DC3) field experiment in 2012 provided a unique opportunity to obtain in situ data related to aerosol properties in the inflow and outflow of convective storms [*Barth et al.*, 2015]. The focus of this work is on two radiatively important properties of aerosol, including hygroscopicity and the real part of the dry particle refractive index. The focus of the hygroscopicity discussion centers around a relative humidity (RH)-independent single parameter value (kappa, κ) often used in models [*Petters and Kreidenweis*, 2007]. As will be further discussed, this parameter relates the aerosol hygroscopic growth factor to RH. The objective of the data analysis is to report on the following: (i) the vertical structure of κ and n based on data for all of DC3 and specifically for the three storm regions probed; (ii) comparison of inflow and outflow data during three case flights with convective storms in contrast to flights with no storms present; (iii) model predictions of aerosol hygroscopicity in the outflow of the three storm case studies when including the effect of entrainment; and (iv) a discussion of factors leading to differences in measured parameters in the PBL versus UT.

2. Experimental Methods

2.1. DC3 Field Campaign

The Deep Convective Clouds and Chemistry (DC3) study was conducted during May and June 2012 using multiple platforms based out of Salina, Kansas. The objective was to study the chemical and transport processes associated with deep convection in midlatitude, continental, deep convective clouds [*Barth et al.*, 2015]. Measurements targeted three regions for sampling thunderstorms: northeastern Colorado, Oklahoma-Texas, and northern Alabama. Three aircraft (i.e., NASA DC-8, NSF/NCAR Gulfstream V (GV), and DLR Falcon 20) flew coordinated flight patterns, sampling inflow and outflow regions of storms to quantify atmospheric composition in and around the storm cells. Ground-based observations monitored storm development, physical structure, and lightning location. The instrumental suite aboard the DC-8, the platform of interest in this study, included instruments to characterize parameters associated with meteorology, radiation, clouds, gases, and aerosol particles.

2.2. DC-8 Measurements

2.2.1. DASH-SP

A key instrument in this study is the Differential Aerosol Sizing and Hygroscopicity Spectrometer Probe (DASH-SP), which measures size-resolved hygroscopic growth factors (GF = ratio of humidified diameter to dry diameter) and the real part of the dry particle refractive index (n) [*Sorooshian et al.*, 2008a]. Instrument operating details, data processing procedures, and examples of its field deployment are presented elsewhere [*Sorooshian et al.*, 2008a, 2008b; *Hersey et al.*, 2009, 2011, 2013; *Shingler et al.*, 2016a], but a brief description is provided here.

On the DC-8, the ambient aerosol stream sampled by the DASH-SP first entered through an isokinetically controlled inlet that efficiently collects and transmits particles smaller than 4 μm diameter [*McNaughton et al.*, 2007]. The air sample is next passed through a nafion dryer (Perma-Pure FC-125-240-10PP) before entering a differential mobility analyzer (DMA) to generate a monodisperse aerosol stream at a chosen dry particle

diameter. That stream is subsequently split to separate dry and humidified streams feeding optical particle counters (OPCs) that are used to quantify the final humidified diameter. The OPCs measure light scattering intensity using diode lasers at a wavelength of 532 nm (World Star Technologies, Model TECGL-30). The OPC in the dry aerosol stream is used to determine n, while the other OPC measures light scattering for particles that have passed through a diffusion-based humidifier. The residence time of sampled aerosol is ~3 s from the entrance of the DASH-SP to the humidifier, followed by another ~4 s from the humidifier to the OPCs. An algorithm is used to quantify GF using knowledge of dry particle diameter, n, and the humidified OPC light scattering distribution [*Shingler et al.*, 2016a].

During DC3, the DASH-SP humidified RH was set to values typically between 70 and 95% with dry measurements below 15%. The dry diameter range was between 180 and 400 nm. Humidity within the DASH-SP humidified channel was controlled within 1.5% RH, and the uncertainty in GF and n measurements is less than 3% and 0.01, respectively [*Sorooshian et al.*, 2008a; *Shingler et al.*, 2016a]. The time resolution of DASH-SP measurements was on the order of seconds in the PBL due to high particle concentrations in the dry diameter range that the DASH-SP can measure. However, in the UT where anvil outflows were present, measurements required a longer amount of time to gather sufficient statistics to robustly derive GF and n as opposed to dividing the data into more data points with less statistical robustness. The average (± standard deviation) time to obtain a single GF and n value for inflow and outflow sampling was 29 ± 5 s and 54 ± 41 s, respectively. Furthermore, for other flights discussed below without storm convection, the times to get a single GF and n data value for low (< 4 km) and high altitude (> 8 km) data reported were 13 ± 11 s and 51 ± 48 s, respectively.

In order to intercompare GF data at the various humidified RHs meaningfully and to still have sufficient statistics for the subsequent analyses presented, GFs were converted to a RH-independent single parameter value (kappa, κ) often used in models [*Petters and Kreidenweis*, 2007]. In the subsaturated regime, κ is directly related to GF using the approximation shown in equation (1) (where RH corresponds to the mole fraction-based water activity in a liquid particle phase in equilibrium with the gas phase).

$$[\mathrm{GF}]^3 = 1 + \kappa \left(\frac{\frac{\mathrm{RH}}{100\%}}{1 - \frac{\mathrm{RH}}{100\%}} \right) \tag{1}$$

2.2.2. Other Instrumentation

The Meteorological Measurement System (MMS) aboard the DC-8 provided measurements of ambient temperature, pressure, horizontal winds, and relative humidity. Ice water content (IWC) data were obtained by a SPEC 2D-S (Stereo) Optical Array Cloud Particle Imaging Probe [*Lawson et al.*, 2006] and were used to classify air as being cloud-free in outflow regions when <0.001 g kg^{-1}. Nonmethane hydrocarbons were measured using the whole air sampler (WAS) coupled offline to gas chromatography [*Colman et al.*, 2001; *Simpson et al.*, 2010]. Carbon monoxide (CO) was measured with a differential absorption mid-IR diode laser spectrometer [*Sachse et al.*, 1991]. Submicrometer aerosol composition, specifically including nonrefractory components, was measured with a High Resolution Aerosol Mass Spectrometer (HR-AMS) [*DeCarlo et al.*, 2006; *Dunlea et al.*, 2009]. Submicrometer black carbon (BC) mass concentration was measured with a Humidified-Dual Single-Particle Soot Photometer (HD-SP2) [*Schwarz et al.*, 2015]. To complement the DASH-SP hygroscopicity data, the ratio of humidified scattering coefficient to dry scattering coefficient at 550 nm, f(RH), for bulk aerosol was measured with the Langley Aerosol Research Group Experiment (LARGE) tandem humidified nephelometers (TSI Inc., Model 3563) [*Ziemba et al.*, 2013]. The f(RH) data were obtained at dry (RH 20%) and humidified (RH 80%) scattering channel settings, and with a reported uncertainty of ±0.05.

2.3. Radar Measurements

Data are used from the Weather Surveillance Radar-1988 Doppler (WSR-88D) System [*Crum and Alberty*, 1993], a product of the Next Generation Weather Radar (NEXRAD) program, to examine storm structure and estimate the distance between the DC-8 and the nearest storm core [*Barth et al.*, 2016; *Fried et al.*, 2016]. Three-dimensional composites were produced from multiple S band (10 cm wavelength) radars following the methodology described in *Homeyer* [2014] and *Homeyer and Kumjian* [2015].
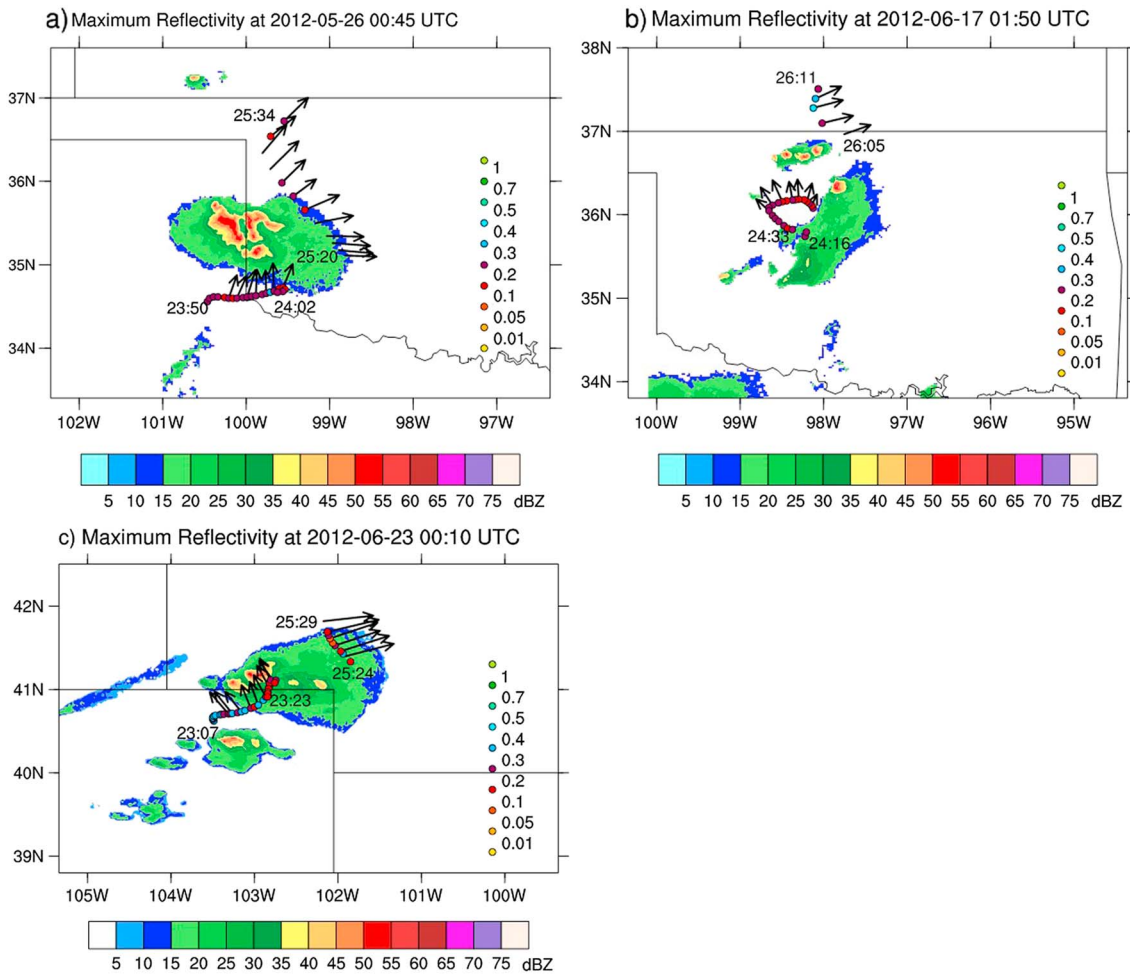
Figure 1. Flight tracks represented by circular markers colored by κ during the periods of time when the DC-8 was sampling inflow and outflow aerosol in the following three storm case flights initiated on the following days: (a) 25 May 2012, (b) 16 June 2012, and (c) 22 June 2012. (Note that the times of the images are near the end of the flights that extended into the following day based on UTC time.) The maximum column reflectivity from the NEXRAD radars is shown with wind vectors marking the time period of inflow and outflow sampling.

2.4. Inflow/Outflow Sampling Determination

Using methods outlined in other DC3 studies [*Barth et al.*, 2016; *Fried et al.*, 2016], inflow and outflow sample periods were identified using aircraft flight tracks, weather radar ensembles, radiosondes, wind direction, storm cell propagation, speed of aircraft and of storm movement, and trace gas and aerosol measurements to determine stability during aircraft flight legs. Three case flights are examined with storm inflow and outflow data (25 May 2012, 16 June 2012, and 22 June 2012) for which a sufficiently high particle number concentration was observed in the DASH-SP size range above 10 km where anvil outflows typically were sampled; other inflow/outflow DC3 flights discussed in other studies [e.g., *Barth et al.*, 2016; *Bela et al.*, 2016; *Corr et al.*, 2016; *Fried et al.*, 2016] are not considered here owing to insufficient DASH-SP statistics available in outflow regions of those flights. The first two storms were in Oklahoma, and the last one was in the vicinity of northeast Colorado and southwest Nebraska (Figure 1). All three storm cases represent severe convection with high convective available potential energy (CAPE) with the following values: 25 May = 3650 J kg^{-1}, 16 June = 3049 J kg^{-1}, and 22 June = 2563 J kg^{-1}. There was also substantial vertical wind shear between 0 and 6 km on these days: 25 May = 13.4 m s^{-1}, 16 June = 15.9 m s^{-1}, and 22 June = 24.2 m s^{-1}. These storm environment parameters were calculated using sounding data with CAPE determined using the mixed layer (i.e., between surface and 100 hPa above surface) mean temperature.

Measurements of inflow and outflow regions of targeted storms were obtained by a precise flight pattern described in other work [*Barth et al.*, 2015, 2016; *Fried et al.*, 2016]. Such flight tracks began with sampling boundary layer inflow composition at a number of altitudes crossing in front of the storm in the PBL and just above the PBL height, then spiraling to the convective anvil outflow region with multiple subsequent flight legs at high altitude. In alignment with methods presented by *Barth et al.* [2016] and *Fried et al.* [2016], measurements taken closest to the storm core top are presented here to minimize biases due to dilution and subsequent out-of-cloud aerosol processing; however, this was typically dozens of kilometers downwind of the storm core top to avoid aircraft damage. Regions of inflow and outflow were determined by analyzing flight legs where horizontal winds indicated air flowing into storm within the PBL for inflow and air flowing from the storm core in the anvil for outflow (Figure 1) [*Barth et al.*, 2016; *Fried et al.*, 2016]. Inflow and outflow times (UTC) of the three case flights are as follows (inflow/outflow): 25 May = 23:53–24:00/25:20–25:34; 16 June: 24:21–24:28/26:05–26:09; and 22 June: 23:10–23:20/25:25–25:29. Based on 48 h back trajectory data from the Hybrid Single-Particle Lagrangian Integrated Trajectory (HYSPLIT) model [*Stein et al.*, 2015; *Rolph*, 2016], the air mass source region impacting the inflow on the three storm days was from the south (Texas, Mexico, and the Gulf Coast).

There is often concern with aerosol data contamination associated with ice shatter on inlets [e.g., *Murphy et al.*, 2004; *Heymsfield*, 2007; *Jensen et al.*, 2009; *Froyd et al.*, 2010; *Lawson*, 2011; *Cziczo and Froyd*, 2014]. As noted by *Corr et al.* [2016] for the DC3 campaign, the inlet used for DASH-SP measurements, which was common to other measurements too, did not exhibit a clear dependence of aerosol parameters (i.e., volume concentration and calcium mass concentration) on either IWC or number concentration of large ice particles (diameter $> 50\,\mu m$), as would be the case in the presence of ice shattering. Owing to the difficulty of the outflow measurements, two of the three storm cases (16 June and 22 June) where DASH-SP data could be obtained coincided with IWC exceeding $0.001\,\mathrm{g\,kg^{-1}}$. IWC data were not available on 25 May; however, forward camera video images suggested that there may have been some cloud affecting at least a subset of the outflow data points. For each of the three storm flights, no relationship was observed in the vicinity of the anvil outflow between either IWC or the forward camera cloud indicator with either κ or n. HR-AMS composition data were also not affected by IWC inlet artifacts.

3. Results

### 3.1. Control Flights and Cumulative Data

To put the storm flight data into context, first we report vertical profiles of κ and n based on cumulative DC3 data and for data in the three main storm regions studied (northeastern Colorado, Oklahoma/Texas, and northern Alabama) (Figure 2). In addition, data are examined from three "control" case flights with both low- and high-altitude data during periods when the DASH-SP did not sample inflow and outflow air from convective storms (Table 1). The control flight data are from areas in Alabama (21 May), Illinois (26 May), and Illinois and Tennessee (30 May). For these three flights, the high-altitude data were above 8 km, with low-altitude measurements below 2 km (except that 30 May was below 4 km). The 26 May and 30 May cases were flights in which the DC-8 was probing convective outflow a day after a previous flight focused on convection; however, the data from the 26 May and 30 May cases used here represent mostly background UT aerosol rather than the outflow and include no data from the previous day of measurements. The data in Figure 2 are for when IWC $< 0.001\,\mathrm{g\,kg^{-1}}$.

The average κ and n values (±1 standard deviation) during DC3 were 0.22 ± 0.10 and 1.50 ± 0.02, respectively. The cumulative vertical profiles of both parameters reveal considerable variability at each altitude relative to the differences in mean values between different altitudes. When comparing only the mean values at each altitude, both κ and n tended to be higher in the lowest 1 km versus the next several kilometers higher in altitude. Interestingly, the mean κ value was highest at the uppermost altitude bin (6.82 ± 1.51 km) for northern Alabama (0.39) as compared to lower altitudes (0.24–0.31). When comparing the three storm regions, mean values of κ and n were higher over northern Alabama, which is consistent with higher sulfate mass fractions (MF_{sulf}) and lower organic mass fractions (MF_{OA}) (Figure 2). A more detailed discussion of chemical relationships with κ and n is in section 4.2.

The average low-/high-altitude values of κ for the three control case flights ranged between 0.20 and 0.23/ 0.18 and 0.25, while n varied between 1.50 and 1.52/1.49 and 1.50. The "high altitude − low altitude"
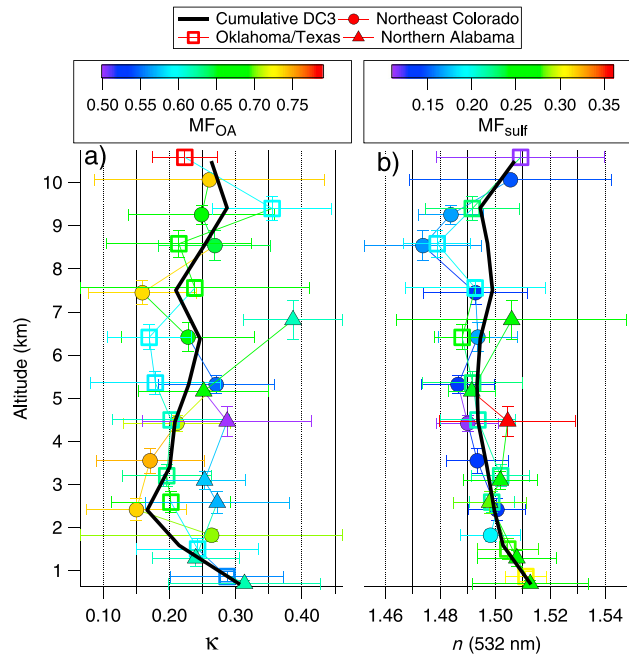
Figure 2. Vertical profiles of (a) hygroscopicity (κ) and the (b) real part of the dry particle refractive index (n) at 532 nm for aerosol in cloud-free air with $D_{p,dry}$ between 180 and 400 nm. Data are shown for cumulative DC3 data and for each of the three major areas examined with storms: northeastern Colorado and southwestern Nebraska (39.2° to 42.0°N, −105.6° to −101.6°W); southwestern Oklahoma and northern Texas (33.8° to 36.7°N, −100.1° to −95.9°W); and northern Alabama and southern Tennessee (33.8° to 35.8°N, −87.7° to −85.6°W). The vertical and horizontal whiskers represent 1 standard deviation.

difference in κ for each case flight ranged between 0.02 and −0.03, with p values exceeding 0.10 when examining the difference in the low/high means for each case based on a two-tailed Student's t test. Interestingly, the lowest p value was for 26 May when κ was lower at high altitude ($p = 0.11$ versus 0.39–0.70 for the other cases). In contrast, values of n were lower at high altitude for all three control cases, and the differences in the means for all but one flight (30 May when $p = 0.11$) were statistically significant with a p value threshold of 0.01. Although the differences in n between the inflow and outflow appear small, even a small change can still lead to a major difference in radiative flux calculations; for example, a 5% change in values of n can translate to a change of 26–32% in the aerosol-induced radiative flux change at the top of the atmosphere [Redemann et al., 2000].

3.2. Storm Convection Flights

Results from the three storm case flights are summarized in Table 2 and further shown in Figure 3 in the case of κ. For one of the three case flights, κ was enhanced for the outflow aerosol as compared to the inflow, with the magnitude of this enhancement being 0.03 (16 June:

Table 1. Summary of Hygroscopicity (κ) and the Real Part of the Dry Particle Refractive Index (n) at 532 nm for Aerosol With $D_{p,dry}$ Between 180 and 400 nm During Control Flights in Which the DASH-SP Did Not Sample Inflow and Outflow Air of Storms[a]

	21 May 2012		26 May 2012		30 May 2012	
	Low	High	Low	High	Low	High
Altitude (km)	1.24 (0.13)	8.77 (0.47)	1.17 (0.26)	10.42 (0.78)	2.97 (0.95)	9.43 (0.05)
κ	0.23 (0.05)	0.25 (0.11)	0.21 (0.06)	0.18 (0.11)	0.20 (0.08)	0.22 (0.07)
n	1.51 (0.01)	1.50 (0.02)	1.52 (0.01)	1.50 (0.02)	1.50 (0.01)	1.49 (0.01)
p value (κ)	0.39		0.11		0.70	
p value (n)	0.01		0.00		0.13	
f(RH)	1.17 (0.08)	1.89 (0.62)	2.07 (0.12)	1.65 (0.67)	NA	NA
MF_{OA}	0.63 (0.04)	0.55 (0.12)	0.60 (0.05)	0.76 (0.07)	0.59 (0.05)	0.58 (0.02)
MF_{sulf}	0.23 (0.03)	0.29 (0.09)	0.27 (0.04)	0.13 (0.06)	0.20 (0.02)	0.24 (0.01)
MF_{nit}	0.04 (0.02)	0.06 (0.02)	0.01 (0.00)	0.05 (0.02)	0.09 (0.03)	0.05 (0.01)
MF_{amm}	0.09 (0.01)	0.08 (0.04)	0.10 (0.01)	0.05 (0.01)	0.11 (0.01)	0.09 (0.00)
MF_{chl}	0.00 (0.00)	0.01 (0.00)	0.00 (0.00)	0.00 (0.00)	0.00 (0.00)	0.00 (0.00)
MF_{BC}	0.01 (0.00)	0.01 (0.01)	0.01 (0.00)	0.01 (0.01)	0.01 (0.00)	0.02 (0.00)
O:C	0.62 (0.03)	0.90 (0.20)	0.65 (0.09)	0.72 (0.13)	0.67 (0.05)	1.08 (0.13)

[a]Data are shown for low and high altitudes. Also shown are p values when comparing means using a two-tailed Student's t test, f(RH) values, chemical mass fractions, and the O:C ratio of organic aerosol. Numbers in parentheses represent 1 standard deviation. The MF parameters correspond to chemical mass fractions for organic aerosol (OA), sulfate (sulf), nitrate (nit), ammonium (amm), chloride (chl), and black carbon (BC). NA: not available.
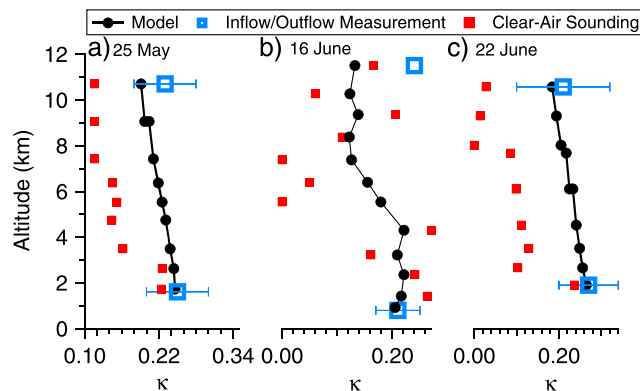
Table 2. Summary of Hygroscopicity (κ) and the Real Part of the Dry Particle Refractive Index (n) at 532 nm for Aerosol With $D_{p,dry}$ Between 180 and 400 nm During Storm Flights in Which the DASH-SP Sampled Inflow and Outflow Air[a]

	25 May 2012		16 June 2012		22 June 2012	
	Inflow	Outflow	Inflow	Outflow	Inflow	Outflow
Altitude (km)	1.62 (0.09)	10.58 (0.19)	0.81 (0.05)	11.26	1.91 (0.00)	10.08 (0.00)
κ	0.25 (0.05)	0.23 (0.05)	0.21 (0.04)	0.24	0.27 (0.07)	0.21 (0.11)
n	1.50 (0.01)	1.51 (0.03)	1.51 (0.01)	1.54	1.50 (0.01)	1.49 (0.02)
p value (κ)		0.65		NA		0.27
p value (n)		0.66		NA		0.24
f(RH)	1.84 (0.04)	1.17 (0.15)	NA	NA	1.47 (0.09)	0.96 (0.16)
MF_{OA}	0.56 (0.01)	0.81 (0.05)	0.60 (0.03)	0.77	0.60 (0.02)	0.74 (0.09)
MF_{sulf}	0.33 (0.01)	0.11 (0.03)	0.27 (0.04)	0.10	0.28 (0.01)	0.10 (0.06)
MF_{nit}	0.01 (0.00)	0.04 (0.00)	0.02 (0.01)	0.07	0.02 (0.01)	0.09 (0.02)
MF_{amm}	0.10 (0.00)	0.04 (0.01)	0.09 (0.01)	0.03	0.10 (0.00)	0.06 (0.01)
MF_{chl}	0.00 (0.00)	0.01 (0.00)	0.00 (0.00)	0.00	0.00 (0.00)	0.01 (0.00)
MF_{BC}	0.01 (0.00)	0.01 (NA)	0.01 (0.00)	0.02	NA	NA
O:C	0.70 (0.02)	0.71 (0.07)	0.60 (0.04)	0.87	0.65 (0.03)	0.49 (0.03)

[a]Also shown are p values when comparing means using a two-tailed Student's t test, f(RH) data, chemical mass fractions, and the O:C ratio of organic aerosol. Numbers in parentheses represent 1 standard deviation. BC data are not used in certain outflows owing to HD-SP2 cloud filters applied.

inflow = 0.21, outflow = 0.24). The outflow data for 16 June coincides with a 2 min sample collected by the DASH-SP; however, it is noted that there were three subsequent data points between 10.4 and 11.1 km that were very close to the anvil, the first two of which may have also been influenced by the outflow of this storm or another storm's outflow with subsequent aging. This is based on comparing the radar reflectivity image in Figure 1 with near-IR satellite image at 26:02 on 16 June. The κ values for those three subsequent points, which coincided with IWC $<$ 0.001 g kg^{-1}, in order of time were 0.49, 0.32, and 0.21. Therefore, including at least the very next sample would have resulted in an even larger κ enhancement in the outflow relative to the inflow. The subsequent discussion considers only the value of the first of the four data points that most confidently was in the outflow.

For 25 May, there was a slight κ reduction in the outflow (inflow = 0.25, outflow = 0.23) with a larger reduction for 22 June (inflow = 0.27, outflow = 0.21). Of note is that the 22 June storm was characterized by influence of biomass burning smoke from the High Park Fire with the smoke being entrained into the storm at an altitude of ~7 km around 00:00 UTC [*Barth et al.*, 2015; *Bela et al.*, 2016]. Owing to the nature of the measurements conducted where more time was spent to collect individual DASH-SP size distributions at high altitude to obtain more statistically robust κ values, p values associated with examining the difference in the means of inflow versus outflow are only as low as 0.27 for the two cases when sufficient data points were available in the outflow to do this calculation (p = 0.65/0.27 for 25 May/22 June, respectively). Had the sampling strategy been to collect more scans with lower particle concentrations, the p value could have been more favorable to show higher significance. We caution that even though the p values are high, the conclusion reached subsequently about how κ is

Figure 3. Vertically resolved κ values for the three storm case flights corresponding to the following: (red) cloud-free average values nearby the storm; (blue) measured inflow and outflow values (whiskers = 1 standard deviation); (black) predicted values in the storm obtained using an altitude-dependent entrainment model.

higher than what an altitude-dependent entrainment model predicts for outflow aerosol particles is robust for all three storm cases.

Differences in n between inflow and outflow conflicted between the three cases. More specifically, n was lower in the outflow of the 22 June case as compared to inflow (1.49 versus 1.50), unlike for 25 May (inflow = 1.50; outflow = 1.51) and 16 June (inflow = 1.51; outflow = 1.54). A notable result, therefore, is that in the absence of storm convection, n is reduced at high altitudes as compared to low altitudes with high statistical significance as compared to cases of storm convection.

4. Discussion

4.1. Entrainment Modeling

To help interpret the measurement data from the three storm flights, it is important to consider the impact of entrainment of cloud-free air into each of the storms examined. A summary of the altitude-dependent entrainment model used for our calculations is described in detail elsewhere [*Barth et al.*, 2016; *Fried et al.*, 2016] and is briefly summarized here. Cloud-free profiles of n-butane, i-butane, n-pentane, and i-pentane were used to calculate entrainment rate while making sure that data with biomass burning and stratospheric influence were omitted. Biomass burning smoke influences were identified based on carbon monoxide (CO) mixing ratios and aircraft location relative to the smoke. Stratospheric air influences were identified based on when the ozone to CO ratio exceeded 1.25, similar to the method of *Hudman et al.* [2007]. It is cautioned though that a finite possibility exists of there still being data points with stratospheric influence due to mixing of air promoted by thunderstorms [e.g., *Schroeder et al.*, 2014]. The model transports a parcel of air from just below cloud base to the anvil outflow measurements. Entrainment rate is calculated using mixing ratios of the various volatile organic compounds (VOCs) listed above in 1 km increments over the course of the parcel trajectory. Sounding measurements of κ in the clear air adjacent to the three storms of focus were used for the entrainment calculations and are visually shown in Figure 3 relative to the model output.

The model results reveal that for all three cases, κ is predicted to be lower in the outflow regions as compared to both the measured inflow and outflow values (Figure 3). For 25 May, the outflow κ is predicted to be 0.191 as compared to the measured value of 0.23. For 16 June, which exhibited an enhancement in measured κ in the outflow (0.24 versus 0.21 in inflow), the predicted value in the outflow is 0.130. The predicted outflow κ value for 22 June was 0.184, in contrast to the measured value of 0.21. A key result of this study is that the mean κ values measured in the outflows of the three cases exceeded the predicted value. This is due to some process(es) that increased κ values during vertical aerosol transport that offset reductions owing to entrainment of cloud-free air. A plausible physical explanation is that there may be extensive aqueous-phase chemistry (i.e., secondary formation of hygroscopic aerosol species, such as sulfate) that acts to enhance the hygroscopicity of the outflow aerosol to the extent that it can offset the reduction owing to entrainment and other effects such as wet scavenging.

With regard to wet scavenging, it is worth noting that previous work investigated aerosol scavenging for a different storm case during DC3 (29–30 May 2012) [*Yang et al.*, 2015]. They reported high scavenging efficiencies $(1 - \frac{\text{Anvil Concentration}}{\text{Anvil Concentration}_{\text{no scavenging}}})$ for both aerosol number (~0.68 for $0.039 \leq D_p \leq 2.5$ μm) and submicrometer aerosol mass (~0.81), and with higher scavenging efficiencies for larger particles (0.156–2.5 μm: 0.84) versus smaller particles (0.039–0.156 μm: 0.64). They observed little chemical selectivity in scavenging between ammonium, sulfate, and organics (0.80–0.84); however, nitrate exhibited reduced scavenging efficiency (0.57) compared to the other species. In the next section we extend the discussion related to aerosol composition.

4.2. Aerosol Composition Results

A primary driver of both κ and n is aerosol composition, and thus, it is imperative to try to explain changes in both parameters between low and high altitudes with available data from the HR-AMS and HD-SP2 instruments. It is cautioned that the DASH-SP data are size-resolved unlike the chemical data. It is generally accepted that increasing (decreasing) organic (inorganic) mass fraction (MF_{OA}) coincides with suppressed hygroscopicity [e.g., *Petters and Kreidenweis*, 2007; *Zieger et al.*, 2015], as has been demonstrated with airborne measurements over the continental United States [*Brock et al.*, 2016; *Shingler et al.*, 2016a].

Furthermore, airborne measurements over the United States have shown that the κ associated with the organic fraction (κ_{OA}) increases as a function of the atomic oxygen-to-carbon ratio (O:C) above values of 0.40 [*Shingler et al.*, 2016a]. Thus, it is of interest to see how well κ and n between different altitudes correlates with MF_{OA} and the O:C ratio of organic aerosol.

4.2.1. Composition Versus Hygroscopicity

For the three control flights, both the low- and high-altitude aerosol were dominated by organics with average MF_{OA} values ranging from 0.59 to 0.63 and 0.55 to 0.76, respectively (Table 1). Sulfate was the next most abundant component with its mass fraction (MF_{sulf}) ranging from 0.13 to 0.29. The most significant change in κ (albeit only by 0.03) was for 26 May when κ was lower at high altitude. MF_{OA} was larger at high altitude (high = 0.76; low = 0.60) without a large difference in the O:C ratio (high = 0.72; low = 0.65). Expectedly, MF_{sulf} was lower at high altitude (high = 0.13; low = 0.27) to compensate for a higher MF_{OA}. Data from 21 May reveal a lower MF_{OA} at high altitudes (0.55 versus 0.63 at low altitude) with a higher O:C ratio (0.90 versus 0.62 at low altitude), which is consistent with a higher κ. The 30 May MF_{OA} values are nearly identical (0.58–0.59) between low and high altitudes, but the MF_{sulf} and O:C ratios were higher aloft (0.24 versus 0.20 and 1.08 versus 0.67, respectively), coinciding with a higher κ.

Similar to the control flights, organics dominated aerosol composition in the storm case flights with MF_{OA} values ranging from 0.56 to 0.60 in inflows and 0.74 to 0.81 in outflows (Table 2). Sulfate was the next most abundant component (MF_{sulf}: 0.10–0.33). MF_{OA} was higher in the outflows for all three flights by between 0.14 and 0.25, while MF_{sulf} was lower in outflows by between 0.17 and 0.22. While the increase (decrease) in MF_{OA} (MF_{sulf}) in the outflow is consistent with κ being lower for at least two of the flights (25 May and 22 June), the κ enhancement in the outflow of 16 June cannot be explained by MF_{OA} and MF_{sulf}, which increased and decreased, respectively, in the outflow. Interestingly, the outflow of 16 June exhibited an enhancement of O:C by 0.27 in the outflow, which can help explain at least some of the enhancement in κ. A comparison to results of *Shingler et al.* [2016a, Figures 10 and 11] of how hygroscopicity varies as a function of O:C ratio over the continental United States reveals that the κ associated with the organic fraction (i.e., κ_{OA}) can increase by between 0.02 and 0.03 for the O:C increase observed on 16 June, but it would be offset in the other direction to a greater extent by the increase in MF_{OA}.

Figure 4a compares κ with both MF_{OA} and MF_{sulf} for the six flights discussed above. When examining all six flights worth of data together, the mass fraction with the strongest relationship with κ was that of sulfate ($r = 0.42$), followed in order by MF_{nit} ($r = -0.32$), MF_{OA} ($r = -0.29$), and the O:C ratio ($r = -0.19$). Because of how the 16 June data do not follow the trend of other flights, the inverse relationship between κ and MF_{OA} is stronger for control flights ($r = -0.76$) versus storm flights ($r = -0.35$), while the relationship between κ and MF_{sulf} is also stronger for control flights ($r = 0.86$ versus 0.44). Aside from the six case flights, when examining the cumulative data from Figure 2 for the three storm regions, κ exhibited similar correlation values with both MF_{OA} ($r = -0.44$) and MF_{sulf} ($r = 0.44$), albeit opposite in sign, with the next strongest correlation being with the O:C ratio ($r = 0.35$).

The 16 June flight is the most challenging case to explain as it is unlikely that an increase of κ by 0.03 can be explained by an increase in the O:C ratio while MF_{org} also increased. As noted earlier, if the subsequent DASH-SP data point ($\kappa = 0.49$) after the main outflow point shown in Table 2 was included, the κ enhancement would have been even larger without any difference in the chemical results as the mass fractions (and O:C ratio) for that next point were nearly identical to the previous point. One potential explanation for the disagreement between the chemical and hygroscopicity data for this specific case could be related to the size-resolved nature of the DASH-SP measurements unlike the chemical data used, which would mean that the intercomparison is not fair.

As an attempt to address this issue, f(RH) data for bulk aerosol were analyzed for flights in which such data were available (Tables 1 and 2). Similar to size-resolved κ data, lower values of f(RH) coincide with higher (lower) MF_{OA} (MF_{sulf}) values. For an extended discussion of the counter-intuitive f(RH) values below unity on 22 June, the reader is referred to *Shingler et al.* [2016b] where it is explained that such data are not uncommon aloft when sampling biomass burning plumes. When considering the four flights in Tables 1 and 2 when f(RH) data were available, f(RH) was best correlated with MF_{sulf} ($r = 0.69$), followed by MF_{OA} ($r = -0.63$) and O:C ($r = 0.60$). Unfortunately, f(RH) data are not available for the critical 16 June case, which is the main
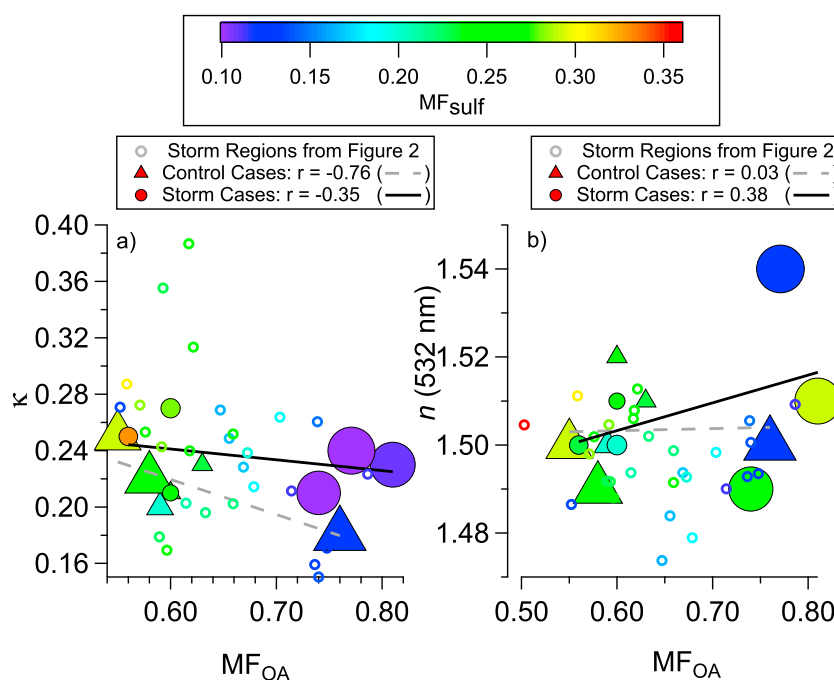
Figure 4. Comparison of κ and n versus MF_{OA} using the high- and low-altitude data from the three control flights in Table 1, inflow/outflow data from the three storm flights in Table 2, and the data from Figure 2 for the three general storm regions probed during DC3. Markers are color coded by the sulfate mass fraction, and sizes of the markers from the six case flights in Tables 1 and 2 are proportional to altitude to differentiate between low- and high-altitude data. Best fit lines are shown for the two sets of points with correlation coefficients (r) reported.

discrepancy between the DASH-SP and composition data; thus, this potential explanation (size-resolved versus bulk data) cannot entirely be ruled out. It is also possible that there may have been influence from species not detectable by the HR-AMS or that MF_{org} is not the most suitable chemical proxy to describe the aerosol hygroscopic behavior. For instance, what could have been influential for the 16 June outflow was the relative amounts of different inorganic species coupled to the increase in the O:C ratio and also nonideal interactions between different aerosol constituents.

4.2.2. Composition Versus Refractive Index

In contrast to the hygroscopicity data, explaining shifts in n values with the composition data is much more challenging for the six case flights summarized in Tables 1 and 2. For instance, there is a consistent reduction in n at high altitudes versus low altitudes in the three control cases, but there was no consistent feature in the chemical data that was distinctly different at high altitudes (Table 1). Similar to the control flights, there is no chemical parameter that matched the changes observed in n across all three storm flights (Table 2). The relationship between n and almost every chemical parameter (except MF_{nit}) was stronger (albeit still weak and sometimes opposite in sign) in the storm case flights as compared to control flights. For example, the correlation between n and various chemical parameters was as follows for storm/control case flights: $MF_{sulf} = -0.34/0.26$, $MF_{amm} = -0.60/0.25$; $MF_{OA} = 0.38/0.03$, O:C $= 0.87/-0.75$, $MF_{nit} = 0.15/-0.67$. When data from the six case flights were combined, n was best correlated with MF_{amm} ($r = -0.39$) followed by MF_{OA} ($r = 0.32$). When examining cumulative data from Figure 2 for the three storm regions, n exhibited its strongest correlation with MF_{nit} ($r = -0.55$) and MF_{sulf} ($r = 0.39$), while one of the weakest relationships was with MF_{OA} ($r = -0.07$). The lack of consistency between composition and n data may be due to different factors that govern n values relative to hygroscopicity, which will be the subject of forthcoming work.

While the DASH-SP cannot quantify the imaginary component of particle refractive index (RI), it is worth noting that the mean single scattering albedo (SSA at 550 nm), as derived from the LARGE package, was between 0.94 and 0.96 for the inflow and outflow of each of the storm cases examined. Values during DC3 were typically in the range of 0.91–0.99, which is representative of more aged particles without very strong absorptive properties as compared to fresh wildfire plumes [*Corr et al.*, 2012, and references therein].

5. Conclusions

Airborne DC-8 data collected during the 2012 DC3 campaign are used in this work to examine the impact of storm convection on subsaturated aerosol hygroscopicity (κ) and the real part of dry aerosol refractive index (n). Three case studies of storm convection are compared with each other and with other flights with high- and low-altitude data without storm convection sampled. The main results are as follows in order of the objectives outlined in section 1:

1. The average κ and n values during DC3 were 0.22 ± 0.10 and 1.50 ± 0.02, respectively. When comparing only the mean values at each altitude, both κ and n tended to be higher in the lowest 1 km versus the next several kilometers higher in altitude. When comparing the three storm regions, κ and n were higher over northern Alabama, which is consistent with higher MF_{sulf} and lower MF_{OA}.
2. Aerosol hygroscopicity in the storm outflow of one case exceeded that of the inflow value (κ: 0.21 to 0.24), while the other two cases exhibited a reduction. While the value of n was higher in the outflow of two of the three storms examined, the values were always lower >8 km on control flights relative to <4 km. Differences in n were more statistically significant on the control flights.
3. For the three storm cases, the mean κ value measured in the outflow exceeds the predicted value based on an altitude-dependent entrainment model that treats mixing of cloud-free air into the storms. This is suggestive of a process such as aqueous-phase chemistry that increases hygroscopicity of convected aerosol in storms even if the outflow κ value is lower in the outflow relative to the inflow.
4. Chemical measurements show that suppressed values of MF_{org} and higher values of MF_{sulf} and the O:C ratio of organic aerosol coincided with higher κ (and $f(RH)$) values, unlike n, when comparing the low- and high-altitude periods during DC3 flights. Differences in n cannot be explained with the available chemical data and requires further research to determine what factors govern its values.

To date there have been limited attempts to quantify how deep convection alters the physicochemical properties of aerosol particles. Since aerosol effects on climate depend on both their radiative properties and vertical distribution, this study demonstrates that deep convection is a critical process to understand as it redistributes particles and changes how they interact with water vapor and solar radiation. Measurements showing that n is reduced in the UT as compared to the PBL on days when storm convection was not targeted is also of critical importance with regard to aerosol radiative forcing calculations, in addition to the use and interpretation of columnar aerosol remote sensing data. This study motivates additional research to investigate both the factors governing n in addition to the relative importance of different in-cloud processes in enhancing outflow aerosol hygroscopicity beyond what an altitude-dependent entrainment model predicts.

References

Ancellet, G., J. L. de Bellevue, C. Mari, P. Nedelec, A. Kukui, A. Borbon, and P. Perros (2009), Effects of regional-scale and convective transports on tropospheric ozone chemistry revealed by aircraft observations during the wet season of the AMMA campaign, *Atmos. Chem. Phys.*, 9(2), 383–411, doi:10.5194/acp-9-383-2009.

Avery, M., et al. (2010), Convective distribution of tropospheric ozone and tracers in the Central American ITCZ region: Evidence from observations during TC4, *J. Geophys. Res.*, 115, D00J21, doi:10.1029/2009JD013450.

Barret, B., et al. (2010), Impact of West African monsoon convective transport and lightning NOx production upon the upper tropospheric composition: A multi-model study, *Atmos. Chem. Phys.*, 10(12), 5719–5738, doi:10.5194/acp-10-5719-2010.

Barth, M. C., S. W. Kim, W. C. Skamarock, A. L. Stuart, K. E. Pickering, and L. E. Ott (2007), Simulations of the redistribution of formaldehyde, formic acid, and peroxides in the 10 July 1996 stratospheric-tropospheric experiment: Radiation, aerosols, and ozone deep convection storm, *J. Geophys. Res.*, 112, D13310, doi:10.1029/2006JD008046.

Barth, M. C., et al. (2015), The deep convective clouds and chemistry (DC3) field campaign, *Bull. Am. Meteorol. Soc.*, 96(8), 1281–1309.

Barth, M. C., et al. (2016), Convective transport and scavenging of peroxides by thunderstorms observed over the central US during DC3, *J. Geophys. Res. Atmos.*, 121, 4272–4295, doi:10.1002/2015JD024570.

Bela, M. M., et al. (2016), Wet scavenging of soluble gases in DC3 deep convective storms using WRF-Chem simulations and aircraft observations, *J. Geophys. Res. Atmos.*, 121, 4233–4257, doi:10.1002/2015JD024623.

Brock, C. A., et al. (2016), Aerosol optical properties in the southeastern United States in summer—Part 1: Hygroscopic growth, *Atmos. Chem. Phys.*, 16(8), 4987–5007, doi:10.5194/acp-16-4987-2016.

Chakraborty, S., R. Fu, J. S. Wright, and S. T. Massie (2015), Relationships between convective structure and transport of aerosols to the upper troposphere deduced from satellite observations, *J. Geophys. Res. Atmos.*, 120, 6515–6536, doi:10.1002/2015JD023528.

Colman, J. J., A. L. Swanson, S. Meinardi, B. C. Sive, D. R. Blake, and F. S. Rowland (2001), Description of the analysis of a wide range of volatile organic compounds in whole air samples collected during PEM-Tropics A and B, *Anal. Chem.*, 73(15), 3723–3731, doi:10.1021/ac010027g.

Corr, C. A., S. R. Hall, K. Ullmann, B. E. Anderson, A. J. Beyersdorf, K. L. Thornhill, M. J. Cubison, J. L. Jimenez, A. Wisthaler, and J. E. Dibb (2012), Spectral absorption of biomass burning aerosol determined from retrieved single scattering albedo during ARCTAS, *Atmos. Chem. Phys.*, 12(21), 10,505–10,518.

Corr, C. A., et al. (2016), Observational evidence for the convective transport of dust over the Central United States, *J. Geophys. Res. Atmos.*, *121*, 1306–1319, doi:10.1002/2015JD023789.

Crosbie, E., J. S. Youn, B. Balch, A. Wonaschutz, T. Shingler, Z. Wang, W. C. Conant, E. A. Betterton, and A. Sorooshian (2015), On the competition among aerosol number, size and composition in predicting CCN variability: A multi-annual field study in an urbanized desert, *Atmos. Chem. Phys.*, *15*(12), 6943–6958, doi:10.5194/acp-15-6943-2015.

Crum, T. D., and R. L. Alberty (1993), The WSR-88D and the WSR-88D operational support facility, *Bull. Am. Meteorol. Soc.*, *74*(9), 1669–1687.

Crumeyrolle, S., L. Gomes, P. Tulet, A. Matsuki, A. Schwarzenboeck, and K. Crahan (2008), Increase of the aerosol hygroscopicity by cloud processing in a mesoscale convective system: A case study from the AMMA campaign, *Atmos. Chem. Phys.*, *8*(23), 6907–6924, doi:10.5194/acp-8-6907-2008.

Cziczo, D. J., and K. D. Froyd (2014), Sampling the composition of cirrus ice residuals, *Atmos. Res.*, *142*, 15–31, doi:10.1016/j.atmosres.2013.06.012.

DeCarlo, P. F., et al. (2006), Field-deployable, high-resolution, time-of-flight aerosol mass spectrometer, *Anal. Chem.*, *78*(24), 8281–8289, doi:10.1021/ac061249n.

Desboeufs, K. V., R. Losno, and J. L. Colin (2001), Factors influencing aerosol solubility during cloud processes, *Atmos. Environ.*, *35*(20), 3529–3537, doi:10.1016/S1352-2310(00)00472-6.

Dunlea, E. J., et al. (2009), Evolution of Asian aerosols during transpacific transport in INTEX-B, *Atmos. Chem. Phys.*, *9*(19), 7257–7287, doi:10.5194/acp-9-7257-2009.

Fried, A., et al. (2016), Convective transport of formaldehyde to the upper troposphere and lower stratosphere and associated scavenging in thunderstorms over the central United States during the 2012DC3 study, *J. Geophys. Res. Atmos.*, *121*, 7430–7460, doi:10.1002/2015JD024477.

Froyd, K. D., D. M. Murphy, P. Lawson, D. Baumgardner, and R. L. Herman (2010), Aerosols that form subvisible cirrus at the tropical tropopause, *Atmos. Chem. Phys.*, *10*(1), 209–218, doi:10.5194/acp-10-209-2010.

Hersey, S. P., A. Sorooshian, S. M. Murphy, R. C. Flagan, and J. H. Seinfeld (2009), Aerosol hygroscopicity in the marine atmosphere: A closure study using high-time-resolution, multiple-RH DASH-SP and size-resolved C-ToF-AMS data, *Atmos. Chem. Phys.*, *9*(7), 2543–2554, doi:10.5194/acp-9-2543-2009.

Hersey, S. P., J. S. Craven, K. A. Schilling, A. R. Metcalf, A. Sorooshian, M. N. Chan, R. C. Flagan, and J. H. Seinfeld (2011), The Pasadena Aerosol Characterization Observatory (PACO): Chemical and physical analysis of the western Los Angeles basin aerosol, *Atmos. Chem. Phys.*, *11*(15), 7417–7443, doi:10.5194/acp-11-7417-2011.

Hersey, S. P., et al. (2013), Composition and hygroscopicity of the Los Angeles aerosol: CalNex, *J. Geophys. Res. Atmos.*, *118*, 3016–3036, doi:10.1002/jgrd.50307.

Heymsfield, A. J. (2007), On measurements of small ice particles in clouds, *Geophys. Res. Lett.*, *34*, L23812, doi:10.1029/2007GL030951.

Homeyer, C. R. (2014), Formation of the enhanced-V infrared cloud-top feature from high-resolution three-dimensional radar observations, *J. Atmos. Sci.*, *71*(1), 332–348, doi:10.1175/JAS-D-13-079.1.

Homeyer, C. R., and M. R. Kumjian (2015), Microphysical characteristics of overshooting convection from polarimetric radar observations, *J. Atmos. Sci.*, *72*(2), 870–891, doi:10.1175/JAS-D-13-0388.1.

Hudman, R. C., et al. (2007), Surface and lightning sources of nitrogen oxides over the United States: Magnitudes, chemical evolution, and outflow, *J. Geophys. Res.*, *112*, D12S05, doi:10.1029/2006JD007912.

Huntrieser, H., et al. (2002), Airborne measurements of NO_x, tracer species, and small particles during the European lightning nitrogen oxides experiment, *J. Geophys. Res.*, *107*(D11), 4113, doi:10.1029/2000JD000209.

Huntrieser, H., H. Schlager, M. Lichtenstern, P. Stock, T. Hamburger, H. Holler, K. Schmidt, H. D. Betz, A. Ulanovsky, and F. Ravegnani (2011), Mesoscale convective systems observed during AMMA and their impact on the NO_x and O_3 budget over West Africa, *Atmos. Chem. Phys.*, *11*(6), 2503–2536, doi:10.5194/acp-11-2503-2011.

Intergovernmental Panel on Climate Change (2013), Summary for policymakers, in *Climate Change 2013: The Physical Science Basis. Contribution of Working Group I to the Fifth Assessment Report of the Intergovernmental Panel on Climate Change*, edited by T. F. Stocker et al., p. 14, Cambridge Univ. Press, Cambridge, U. K.

Jaeglé, L., et al. (1997), Observed OH and HO_2 in the upper troposphere suggest a major source from convective injection of peroxides, *Geophys. Res. Lett.*, *24*(24), 3181–3184, doi:10.1029/97GL03004.

Jensen, E. J., et al. (2009), On the importance of small ice crystals in tropical anvil cirrus, *Atmos. Chem. Phys.*, *9*(15), 5519–5537, doi:10.5194/acp-9-5519-2009.

Lawson, R. P. (2011), Effects of ice particles shattering on the 2D-S probe, *Atmos. Meas. Tech.*, *4*(7), 1361–1381, doi:10.5194/amt-4-1361-2011.

Lawson, R. P., D. O'Connor, P. Zmarzly, K. Weaver, B. Baker, Q. X. Mo, and H. Jonsson (2006), The 2D-S (Stereo) probe: Design and preliminary tests of a new airborne, high-speed, high-resolution particle imaging probe, *J. Atmos. Oceanic Technol.*, *23*(11), 1462–1477, doi:10.1175/JTECH1927.1.

Levin, Z., E. Ganor, and V. Gladstein (1996), The effects of desert particles coated with sulfate on rain formation in the eastern Mediterranean, *J. Appl. Meteorol.*, *35*(9), 1511–1523, doi:10.1175/1520-0450(1996)035<1511:TEODPC>2.0.CO;2.

McNaughton, C. S., et al. (2007), Results from the DC-8 Inlet Characterization Experiment (DICE): Airborne versus surface sampling of mineral dust and sea salt aerosols, *Aerosol Sci. Technol.*, *41*(2), 136–159, doi:10.1080/02786820601118406.

Murphy, D. M., D. J. Cziczo, P. K. Hudson, D. S. Thomson, J. C. Wilson, T. Kojima, and P. R. Buseck (2004), Particle generation and resuspension in aircraft inlets when flying in clouds, *Aerosol Sci. Technol.*, *38*(4), 400–408.

Petters, M. D., and S. M. Kreidenweis (2007), A single parameter representation of hygroscopic growth and cloud condensation nucleus activity, *Atmos. Chem. Phys.*, *7*(8), 1961–1971, doi:10.5194/acp-7-1961-2007.

Pickering, K. E., A. M. Thompson, R. R. Dickerson, W. T. Luke, D. P. McNamara, J. P. Greenberg, and P. R. Zimmerman (1990), Model-calculations of tropospheric ozone production potential following observed convective events, *J. Geophys. Res.*, *95*(D9), 14,049–14,062, doi:10.1029/JD095iD09p14049.

Pickering, K. E., A. M. Thompson, J. R. Scala, W. K. Tao, R. R. Dickerson, and J. Simpson (1992), Free tropospheric ozone production following entrainment of urban plumes into deep convection, *J. Geophys. Res.*, *97*(D16), 17,985–18,000, doi:10.1029/92JD01716.

Redemann, J., et al. (2000), Retrieving the vertical structure of the effective aerosol complex index of refraction from a combination of aerosol in situ and remote sensing measurements during TARFOX, *J. Geophys. Res.*, *105*(D8), 9949–9970, doi:10.1029/1999JD901044.

Ridley, B., et al. (2004), Convective transport of reactive constituents to the tropical and rigid-latitude tropopause region: I. Observations, *Atmos. Environ.*, *38*(9), 1259–1274, doi:10.1016/j.atmosenv.2003.11.038.

Rolph, G. D. (2016), Real-time environmental applications and display system (ready). [Available at http://ready.arl.noaa.gov/.]

Sachse, G. W., J. E. Collins, G. F. Hill, L. O. Wade, L. G. Burney, and J. A. Ritter (1991), Airborne tunable diode-laser sensor for high-precision concentration and flux measurements of carbon-monoxide and methane, *Meas. Atmos. Gases*, *1433*, 157–166.

Schroeder, J. R., L. L. Pan, T. Ryerson, G. Diskin, J. Hair, S. Meinardi, I. Simpson, B. Barletta, N. Blake, and D. R. Blake (2014), Evidence of mixing between polluted convective outflow and stratospheric air in the upper troposphere during DC3, *J. Geophys. Res. Atmos.*, *119*, 11,477–11,491, doi:10.1002/2014JD022109.

Schwarz, J. P., A. E. Perring, M. Z. Markovic, R. S. Gao, S. Ohata, J. Langridge, D. Law, R. McLaughlin, and D. W. Fahey (2015), Technique and theoretical approach for quantifying the hygroscopicity of black-carbon-containing aerosol using a single particle soot photometer, *J. Aerosol Sci.*, *81*, 110–126, doi:10.1016/j.jaerosci.2014.11.009.

Shingler, T., et al. (2016a), Airborne characterization of subsaturated aerosol hygroscopicity and dry refractive index from the surface to 6.5 km during the SEAC[4]RS campaign, *J. Geophys. Res. Atmos.*, *121*, 4188–4210, doi:10.1002/2015JD024498.

Shingler, T., et al. (2016b), Ambient observations of hygroscopic growth factor and *f*(RH) below 1: Case studies from surface and airborne measurements, *J. Geophys. Res. Atmos.*, *121*, 13,661–13,677, doi:10.1002/2016JD025471.

Simpson, I. J., et al. (2010), Characterization of trace gases measured over Alberta oil sands mining operations: 76 speciated C_2–C_{10} volatile organic compounds (VOCs), CO_2, CH_4, CO, NO, NO_2, NO_y, O_3 and SO_2, *Atmos. Chem. Phys.*, *10*(23), 11931–11954, doi:10.5194/acp-10-11931-2010.

Singh, H. B., et al. (2007), Reactive nitrogen distribution and partitioning in the North American troposphere and lowermost stratosphere, *J. Geophys. Res.*, *112*, D12S04, doi:10.1029/2006JD007664.

Sorooshian, A., S. Hersey, F. J. Brechtel, A. Corless, R. C. Flagan, and J. H. Seinfeld (2008a), Rapid, size-resolved aerosol hygroscopic growth measurements: Differential aerosol sizing and hygroscopicity spectrometer probe (DASH-SP), *Aerosol Sci. Technol.*, *42*(6), 445–464.

Sorooshian, A., S. N. Murphy, S. Hersey, H. Gates, L. T. Padro, A. Nenes, F. J. Brechtel, H. Jonsson, R. C. Flagan, and J. H. Seinfeld (2008b), Comprehensive airborne characterization of aerosol from a major bovine source, *Atmos. Chem. Phys.*, *8*(17), 5489–5520.

Sorooshian, A., T. Shingler, A. Harpold, C. W. Feagles, T. Meixner, and P. D. Brooks (2013), Aerosol and precipitation chemistry in the southwestern United States: Spatiotemporal trends and interrelationships, *Atmos. Chem. Phys.*, *13*(15), 7361–7379, doi:10.5194/acp-13-7361-2013.

Stein, A. F., R. R. Draxler, G. D. Rolph, B. J. B. Stunder, M. D. Cohen, and F. Ngan (2015), NOAA's HYSPLIT atmospheric transport and dispersion modeling system, *Bull. Am. Meteorol. Soc.*, *96*(12), 2059–2077.

Sullivan, R. C., S. A. Guazzotti, D. A. Sodeman, and K. A. Prather (2007), Direct observations of the atmospheric processing of Asian mineral dust, *Atmos. Chem. Phys.*, *7*, 1213–1236, doi:10.5194/acp-7-1213-2007.

Wonaschütz, A., et al. (2013), Hygroscopic properties of smoke-generated organic aerosol particles emitted in the marine atmosphere, *Atmos. Chem. Phys.*, *13*(19), 9819–9835, doi:10.5194/acp-13-9819-2013.

Wurzler, S., T. G. Reisin, and Z. Levin (2000), Modification of mineral dust particles by cloud processing and subsequent effects on drop size distributions, *J. Geophys. Res.*, *105*(D4), 4501–4512, doi:10.1029/1999JD900980.

Yang, Q., et al. (2015), Aerosol transport and wet scavenging in deep convective clouds: A case study and model evaluation using a multiple passive tracer analysis approach, *J. Geophys. Res. Atmos.*, *120*, 8448–8468, doi:10.1002/2015JD023647.

Yin, Y., S. Wurzler, Z. Levin, and T. G. Reisin (2002), Interactions of mineral dust particles and clouds: Effects on precipitation and cloud optical properties, *J. Geophys. Res.*, *107*(D23), 4724, doi:10.1029/2001JD001544.

Zieger, P., et al. (2015), Low hygroscopic scattering enhancement of boreal aerosol and the implications for a columnar optical closure study, *Atmos. Chem. Phys.*, *15*(13), 7247–7267, doi:10.5194/acp-15-7247-2015.

Ziemba, L. D., et al. (2013), Airborne observations of aerosol extinction by in situ and remote-sensing techniques: Evaluation of particle hygroscopicity, *Geophys. Res. Lett.*, *40*, 417–422, doi:10.1029/2012GL054428.